

A validated reduced-order dynamic model of nitric oxide regulation in coronary arteries

Hossein Moshfegh^a, Farshad Tajeddini^b, Hossein Ali Pakravan^{a,*}, Mojtaba Mahzoon^a, Ehsan Azadi Yazdi^a, Hamed Bazrafshan Drissi^c

^a School of Mechanical Engineering, Shiraz University, Shiraz, Iran

^b Center of Excellence in Energy Conversion, School of Mechanical Engineering, Sharif University of Technology, Tehran, Iran

^c Cardiovascular Department, Shiraz University of Medical Science, Shiraz, Iran

ARTICLE INFO

Keywords:

Coronary arteries
Nitric oxide regulation
Endothelial cell
Cardiac pacing
Lumped parameter models (LPM)
Dynamic model

ABSTRACT

Nitric Oxide (NO) provides myocardial oxygen demands of the heart during exercise and cardiac pacing and also prevents cardiovascular diseases such as atherosclerosis and platelet adhesion and aggregation. However, the direct in vivo measurement of NO in coronary arteries is still challenging. To address this matter, a mathematical model of dynamic changes of calcium and NO concentration in the coronary artery was developed for the first time. The model is able to simulate the effect of NO release in coronary arteries and its impact on the hemodynamics of the coronary arterial tree and also to investigate the vasodilation effects of arteries during cardiac pacing. For these purposes, flow rate, time-averaged wall shear stress, dilation percent, NO concentration, and Calcium (Ca²⁺) concentration within coronary arteries were obtained. In addition, the impact of hematocrit on the flow rate of the coronary artery was studied. It was seen that the behavior of flow rate, wall shear stress, and Ca²⁺ is biphasic, but the behavior of NO concentration and the dilation percent is triphasic. Also, by increasing the Hematocrit, the blood flow reduces slightly. The results were compared with several experimental measurements to validate the model qualitatively and quantitatively. It was observed that the presented model is well capable of predicting the behavior of arteries after releasing NO during cardiac pacing. Such a study would be a valuable tool to understand the mechanisms underlying vessel damage, and thereby to offer insights for the prevention or treatment of cardiovascular diseases.

1. Introduction

Nitric Oxide (NO), through relaxing vascular smooth muscle cells, plays a fundamental biological role in the modulation of microvascular tone and regional blood flow [1,2]. NO is produced through either purinergic signaling in the vasculature at the cellular scale or as a consequence of the exposure of the endothelial cells to mechanical forces [3]. In fact, shear stress acts as a mechanical stimulus of endothelial cells and triggers a complex cascade of biological events and biochemical reactions leading to an increase in NO level [4]. Consequently, an increase in the diameter of vessel by relaxing vascular smooth muscle cells (VSMCs) ensues [5].

The release of NO is of great importance in the human coronary artery since it helps to provide myocardial oxygen demand of the heart during exercise and cardiac pacing [6]. Besides, it prevents

cardiovascular diseases such as atherosclerosis and platelet adhesion and aggregation [7,8]. Moreover, it has been proven that NO is a determining factor in regulating blood pressure. Thus, impairment of NO bioavailability, which leads to endothelial dysfunction, plays a pivotal role in arising hypertension. Also, Impaired NO bioactivity increases arterial stiffness, which is the main mechanism of systolic hypertension [9]. As a result, it is highly important to investigate the contribution of nitric oxide to human coronary epicardial and microvascular dilation during conditions of increasing myocardial oxygen requirements. For this purpose, several clinical studies have been conducted [10–16]. For instance, Quyyumi et al. [10] have evaluated the coronary microvascular resistance, coronary blood flow, and epicardial diameter, during rest and cardiac pacing. In addition, Nishikawa et al. [11] have investigated the role of endothelium-dependent vascular regulation in patients with and without coronary artery stenosis during

* Corresponding author. Shiraz University, Shiraz, Iran.

E-mail addresses: Moshfegh94.hossein@gmail.com (H. Moshfegh), farshad.tajeddini@gmail.com (F. Tajeddini), pakravan@shirazu.ac.ir (H.A. Pakravan), mahzoon@shirazu.ac.ir (M. Mahzoon), ehsanazadi@shirazu.ac.ir (E. Azadi Yazdi), hamedbazrafshan@yahoo.com (H. Bazrafshan Drissi).

<https://doi.org/10.1016/j.combiomed.2021.104958>

Received 20 June 2021; Received in revised form 30 September 2021; Accepted 16 October 2021

Available online 19 October 2021

0010-4825/© 2021 Elsevier Ltd. All rights reserved.

rest and cardiac pacing, by measuring the left anterior descending (LAD) diameter and its flow rate. Green et al. [12] have shown that by increasing the heart rate and the level of NO during cardiac pacing, no significant changes in pulse pressure can be observed. Levine et al. [15] have stated that NO has a crucial role in modulating the total body energy during exercise. Hoiland et al. [16] have proven that by increasing the hematocrit in arteries, the NO level, and thereby blood flow rate reduces.

Despite the importance of the role of NO in arteries, the direct in vivo study is challenging since the half-life of NO in blood flow is very short [17]. Therefore, NOx, which is the concentration of NO's metabolites is often measured in vivo as the indicator of NO concentration [18]. Yet, Luiking et al. [18] have claimed that NOx may underestimate the NO production since NO production may be under the impact of several factors, including altered renal function, extracellular volume changes, or delayed conversion of NO to nitrate. Other efforts to measure the NO level are limited to animal tests or by using cell culture methods, all of which include highly invasive procedures [19–23]. For instance, Butler et al. [21] studied the impact of step and ramp-induced shear stresses on the arteriolar dilation of an excised arteriole of a rat. Corson et al. [22] investigated the effects of two different paths, meaning calcium-dependent and calcium-independent, on the NO release to show which one plays a dominant role. For this purpose, they cultured aortic endothelial cells (BAEC) and measured NO release under different circumstances [22]. They showed that NO is dominantly released in response to the calcium-independent path. However, since the calcium concentration also affects the NO level, Blackman et al. [23] have studied the effects of different temporal gradients as well as values of shear stress on the consequent response of intracellular calcium concentration. For this purpose, they scraped the endothelial cells of the luminal surface of the calf's ascending aorta after collagen injection and grew them in a specific media. Corson et al. [22] performed the same investigation on the bovine aorta.

Due to the lack of in vivo studies on human to measure the exact level of NO, mathematical models of human vessels have been developed to non-invasively investigate the release of nitric oxide in human vessels [24–30]. Koenigsberger et al. [24] proposed a model for the vessel to investigate the effect of shear stress and blood pressure on the vasomotion. The model considers the change in vessel diameter and the dynamics of calcium concentration within the endothelial cells. Lanzarone et al. [27] proposed an analytical model, based on experimental data, in the Laplace transform domain to study the production of nitric oxide from the endothelium in response to wall shear stress. In this study, the model of nitric oxide regulation in the endothelial layer is based on the hypothesis proposed by Kushan and Frangos [28], in which nitric oxide in the endothelial layer is produced in two parallel paths: calcium-dependent pathway and calcium-independent pathway. Plata et al. [29] proposed a computational model for shear stress-induced nitric oxide production and transport within a parallel flow chamber covered by endothelial cells. Their results revealed the role of convective flow on the transfer of nitric oxide in the flow chamber. Takarada et al. [30] performed simultaneous measurement of the maximum mean velocity of blood in the LAD artery and the change in plasma nitric oxide. Wang et al. [31] proposed a mathematical model to quantitatively assess the pulsatility impact of blood flow on the nitric oxide regulation of the microvasculature. They also indicated that the vascular dilation, due to the nitric oxide production, acts as feedback in the vascular hemodynamic regulation loop. Moreover, Qian et al. [32] developed an MRI-based CFD model to calculate the distribution of NO on the endothelial surface in the carotid artery bifurcations which had atherosclerotic plaque. Their results indicated that atherosclerotic compounds mainly determine the NO concentrations on carotid arteries. Ma et al. [33] developed an analytical model of the Flow Mediated Dilation (FMD) process in combination with nitric oxide, using mathematical modeling with physiological measurements. Their results showed the possibility of using the fractional flow-mediated dilatation (FFMD)

parameter to differentiate the endothelial function between young and middle age groups. Also, in another study, Haselden et al. [34] showed that both the spatial location of NO production and the size of the vessel play an important role in determining its response to NO. They also showed that changes in blood flow during hypoxia or hyperoxia could indicate a decrease in NO in the parenchyma.

Regarding the above review and to the best of our knowledge, a numerical model has not yet been developed for the investigation of NO effect in human coronary arteries. Due to the importance of this issue, this study attempts to model the effect of NO release in coronary arteries and its impact on the hemodynamics of the coronary arterial tree. Moreover, the novelty of the current study is to investigate the vasodilation effects of arteries, as the decisive factor of blood flow and blood pressure, on the hemodynamics of the coronary artery during cardiac pacing. To this end, a mathematical model for dynamic changes of calcium and NO concentration in the coronary artery is developed. The proposed model can be used for further investigation of NO release in the human coronary arteries with stenosis. Such a study would be a valuable tool to understand the mechanisms underlying vessel damage, and thereby to offer insights for the prevention or treatment of cardiovascular diseases.

2. Materials and methods

2.1. 0D model of systemic and pulmonary circuits

The model used here is based on the cardiovascular model presented by Avazolini et al. [35], which is depicted in Fig. 1 (lower panel). It should be mentioned that in circuit and during systole, the driving pressure to supply blood to the myocardium is equal to the difference between the aortic pressure and the left main coronary artery pressure. During diastole, blood is flown into the coronary arteries, by the pressure difference of the aorta and the right atrium. To consider this particular feature in coronary arteries the model is modified by an intramyocardial pressure source (LVP) to take into account the pressure inside the heart during the cardiac cycle. The LVP pressure source has the same value and phase as pressure in the left ventricle. Details of systemic and pulmonary circulation dynamics can be found in Appendix A.

2.2. 0D model of left coronary artery

The coronary arterial model is based on a realistic anatomical geometry of left coronary arteries provided by Scanlon et al. [36], Wang et al. [37], and Pietrabissa et al. [38] (Fig. 1 (upper panel)).

The left main coronary artery originates from the root of the aorta which branches to the left anterior descending (LAD) and left circumflex artery (LCX). The branches from the LAD are labelled in sequence diagonal 1 and diagonal 2. Similarly, branches from LCX are labelled marginal and numbered in order. Based on the concept of the lumped parameter model (LPM), each vessel compartment is replaced by a resistance, capacitance and inductance in series which is depicted in Fig. 1. The electrical potential or voltage (V) corresponds to the driving pressure difference (Δp) in the vessel segment, current (I) is analogous to the blood flow (q), resistor is represented as viscous flow resistance, capacitance is analogous to the compliance of the vessel (C), and inductor is replaced by blood inertia (L). Each element of the electrical circuit can be related to the anatomic property of LPM of coronary compartments as follows [39]:

$$\dot{q}_{in} = \frac{p_{in}}{L} - \frac{p_{out}}{L} - \frac{R}{L} q_{in} \quad (1)$$

$$\dot{p}_{out} = \frac{q_{in}}{C} - \frac{q_{out}}{C} \quad (2)$$

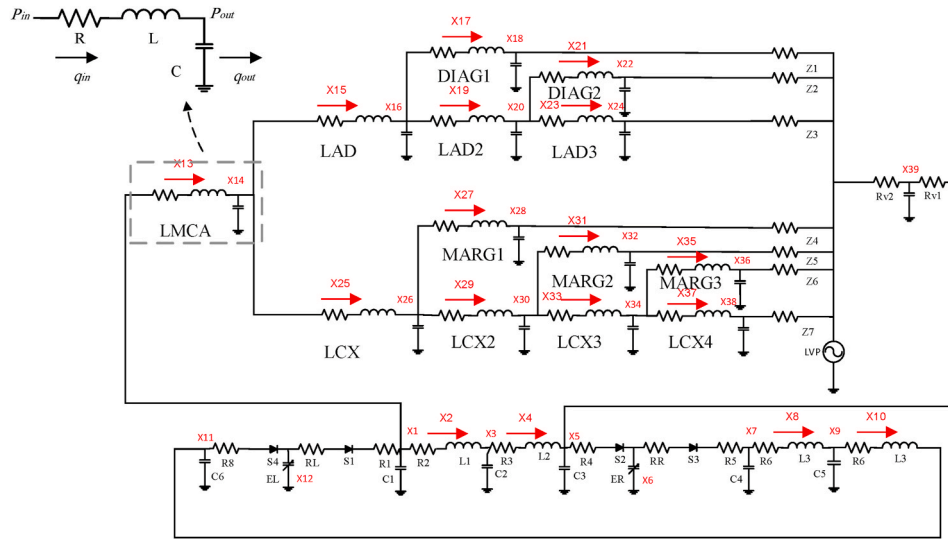


Fig. 1. The considered cardiovascular model, including systemic circulation, pulmonary circulation, coronary circulation, right and left ventricles.

$$R = \frac{128\mu l}{\pi D^4} \quad L = \frac{4\rho l}{\pi D^2} \quad C = \frac{\pi D^2 l}{4} C_{norm} \quad (3)$$

In the aforementioned equations, D , L , and C_{norm} are diameter, vessel length, and average vessel distensibility, respectively. C_{norm} was considered to be $0.002 \text{ [mmHg}^{-1}]$ according to a suggestion by Pagiatakis et al. [39]. Also, p_{in} , p_{out} , q_{in} , and q_{out} are the upstream and downstream pressures and flow rates, respectively. In Eqs. (1) and (2), R , L and C values for each vessel are calculated using Eq. (3) according to their relevant length and diameter in rest and pacing conditions; assuming ρ is the blood density (1060 kg m^{-3}) and μ is the blood viscosity (0.0035 Pa s) [40,41].

At each end of the seven coronary branches shown in Fig. 1, there is a terminal resistance Z corresponding to the capillary resistance in the myocardial tissue. This resistance is calculated by Ref. [39]:

$$Z_{term} = R_{tot} \left[\frac{D_{term}}{D_{LMCA}} \right]^{-5/3} \quad (4)$$

Where Z_{term} , D_{term} , and R_{tot} are the terminal resistances of each branch, the diameter of the terminal epicardial branch [mm], and the

total hypermetric resistance, respectively.

2.3. Dynamic model for vasodilation

The rate at which nitric oxide is released from endothelial cells depends on the wall shear stress [42]. Shear stress, as the input of the nitric oxide regulation model, is obtained from Poiseuille flow assumption as follows [39]:

$$\tau = \frac{32\mu q}{\pi D^3} \quad (5)$$

According to experimental studies [28], nitric oxide is generated simultaneously by two pathways. Fig. 2 shows the block diagram of the NO regulation model.

The calcium-dependent pathway (Fig. 2 (a)) activates after a slight increase in endothelial shear stress [31]. The most prominent feature of this route is the increase in the concentration of cytoplasmic calcium ions. The response to this elevated calcium concentration lasts from a few seconds to about 30 min, depending on the amount of shear stress

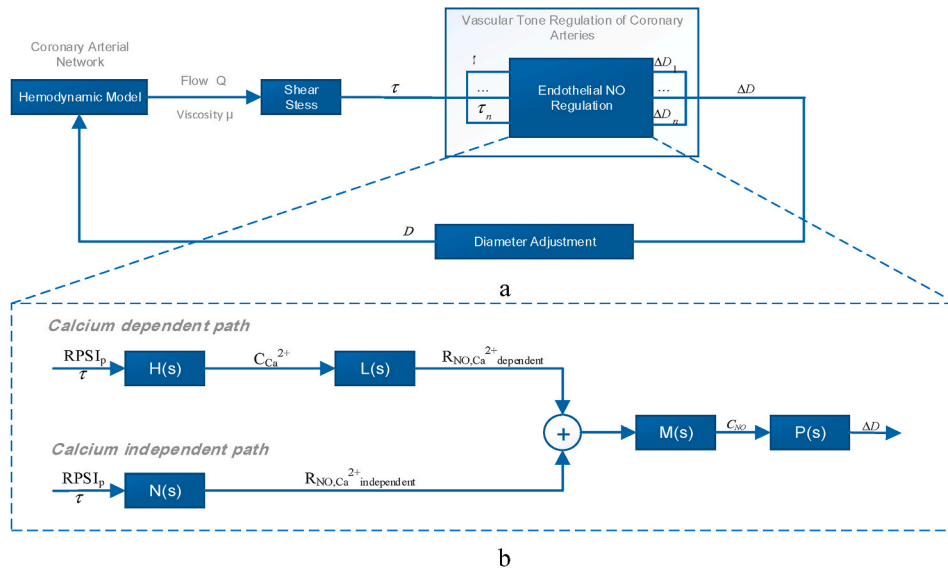


Fig. 2. The block diagram of the NO regulation model; a) The hemodynamic model of flow distribution of coronary arteries and b) The block diagram of Calcium-dependent/independent pathways to produce nitric oxide.

[43]. In contrast, in the calcium-independent pathway (Fig. 2 (b)), NO is released with a time delay relative to the previous state by long-acting synthase production [44]. The NO release and consequent vascular radius variation are described using stable Laplace domain linear transfer functions which were introduced by Lanzaron et al. [27].

2.3.1. Model of the calcium concentration

The transfer function $H(s)$ describes the direct relationship between wall shear stress and calcium concentration C_{Ca}^{2+} (nM) of endothelial layer [31]:

$$H(s) = K_1(\tau) \frac{1.619 \times 10^{-2} [s + 7.486 \times 10^{-3} (1 + z_H)]}{1 + 36.76s + 81.07s^2} \quad (6)$$

Where:

$$K_1(\tau) = \frac{1}{[1 + 115 \exp[-0.5 \cdot \tau]]} \cdot \frac{2 \times 10^5}{\tau} \quad (7)$$

$$z_H = 0.0904 \cdot \exp \left[- \left(\frac{RPSI_P - 4.42}{2.579} \right)^2 \right] \quad (8)$$

In the above equations, τ is the wall shear stress in dyn/cm² and $RPSI_P$ is an indicator of the relative pulse slope index of pressure. It should be mentioned that the best discrimination between arteries and veins is the greatest pulsatile increase in shear rate relative to the time-averaged shear rate in the same vessel. For this study, $RPSI_P$ was chosen to be 17.3 [37].

It should be mentioned that the transfer functions are linear functions in basis. Thus, it was rational to use a linear model to investigate the release of NO. There was the reason the model provided by Wang et al. [31] has been used in this study.

2.3.2. Model of the NO production rate in calcium-dependent pathway

The transfer function $L(s)$ in Eq. (9) expresses the relationship between calcium concentration and calcium-dependent nitric oxide production rate $R_{NO, Calcium-dependent}$ in Ref. nM/s [31]:

$$L(s) = 250.2 \times \frac{-2.945 \times 10^{-7} + 7.084 \times 10^{-4}s + 2.642 \times 10^{-2}s^2 + 5.83 \times 10^{-2}s^3}{1.212 \times 10^{-4} + 4.54 \times 10^{-2}s + 5.659s^2 + 2.349 \times 10^2s^3} \quad (9)$$

2.3.3. Model of the NO production rate in calcium-independent pathway

The transfer function $N(s)$ in Eq. (10) expresses the relationship between shear stress and nitric oxide production rate of calcium-independent pathway $R_{NO, Calcium-independent}$ in nM/s [31]:

$$N(s) = K_2(\tau) \frac{-2.143 \times 10^{-4} [s - 1.432 \times 10^{-2} (1 + z_N)]}{1 + 2.864 \times 10^2s + 2.050 \times 10^4s^2} \quad (10)$$

Where

$$K_2(\tau) = \left[2.13 + \frac{457.5 \cdot \tau}{\tau + 35} \right] \frac{3 \times 10^5}{\tau} \quad (11)$$

$$z_N = \frac{0.102}{1 + 237 \times \exp(-1.179 \times RPSI_P)} \quad (12)$$

2.3.4. Model of the NO concentration

The transfer function $M(s)$ in Eq. (13) describes the relationship between total NO production rate and vascular NO concentration C_{NO} in nM [31]:

$$M(s) = \frac{\alpha \cdot R_{O_2}}{s + \lambda_{tot}} \quad (13)$$

$$R_{NO} = \alpha \cdot R_{O_2} \cdot (R_{NO, Calcium-dependent} + R_{NO, Calcium-independent}) \quad (14)$$

$$R_{O_2} = \frac{P_{O_2}}{P_{O_2} + K_m} \quad (15)$$

$$\lambda_{tot} = \lambda_{tot}^{H_d=0.45} \cdot \frac{H_d}{0.45} \quad (16)$$

Here, α is the adjustment coefficient, R_{O_2} is the oxygen-dependent adjustment function, λ_{tot} is NO scavenging rate, P_{O_2} is the partial pressure of oxygen, K_m is the Michaelis-Menten constant and H_d is the hematocrit. Also, the rate of NO production is a function of the total rate of produced nitric oxide in cultured endothelial cells ($R_{NO, Ca^{2+} dependent} + R_{NO, Ca^{2+} independent}$). The values of α , K_m and $\lambda_{tot}^{H_d=0.45}$ are listed in Table 1.

2.3.5. Model of the vascular dilation

For the transfer function expressing the relationship of NO concentration and vascular dilation ΔD , we have used an existing transfer function studied by Lanzarone et al. [27] which is based on experimental data provided by Bohlen et al. [46]. Since this transfer function is not provided for the coronary artery it should be modified. This is done based on the experimental data provided by Quyyumi et al. [10] in the transfer function $\bar{P}(s)$ and coefficients were adjusted to produce approximately 8% of dilation for the LAD artery during cardiac pacing:

$$\bar{P}(s) = \frac{6.523 \times 10^{-3} + 8.287s + 2.492 \times 10^3s^2 + 8.667 \times 10^4s^3}{3.111 \times 10^{-6} + 1.952 \times 10^{-3}s + 4.015 \times 10^{-1}s^2 + 2.718 \times 10^1s^3} \quad (17)$$

$$K_3(NO) = (0.1047 \times C_{NO} + 0.13) \times 10^{-4} / 250 \quad (18)$$

$$P(s) = K_3(NO) \cdot \bar{P}(s) \quad (19)$$

$$D = D_{initial} \cdot (1 + \Delta D) \quad (20)$$

In the above equations, C_{NO} is the NO concentration and ΔD is vascular dilation percentage.

2.4. Simulation

2.4.1. Rest condition

For mathematical modeling of rest condition, the left and right ventricular pressures, were chosen in such a way as to produce an aortic pressure of 115/70 mm Hg (average pressure is 92) [11]. These pressures are associated with time-varying elastance functions as the main source of driving pressure of the arterial analog network. In addition, the heart-beat was assumed to be 75 bpm [11]. These data were adapted to mimic the condition of patients in the work by Nishikawa et al. [11]. For the rest condition, the values of resistances, compliances, and inductances of each compartment in the coronary part of the circuit were calculated using equations (1)–(3) based on the diameters and lengths of the relevant vessels.

In addition, to calculate terminal resistances (Z), R_{tot} was estimated by assuming a direct relationship between the pressure drop and the flow. In this regard, using Hagen-Poiseuille equation, it was assumed that the total average myocardial flow is 2.2 ml/s in the left main coronary artery (based on a total average resting flow of 1.1 ml/s in LAD and LCX) [47], and the average pressure drop is 87 mmHg (based on the aortic and venous pressures of 92 mmHg and 5 mmHg [39], respectively). It should be mentioned that to model the rest condition, the

Table 1
The constant values in this study.

Parameter	Value	Reference
α	563.2	Wang et al. [31]
K_m	4.7 mm Hg	Wang et al. [31]
$\lambda_{tot}^{H_d=0.45}$	540 s ⁻¹	Lamkin-Kennard et al. [45]

values of resistances and compliances for systemic and pulmonary circulation were obtained from the work by Pagiatakis et al. [39].

The governing ordinary differential equations for pressures and flows of different branches of the coronary arterial network were coupled with cardiovascular governing equations to describe the hemodynamic behavior of the whole cardiovascular network by a system of ODE as follows:

$$\frac{dx_j}{dt} = \varphi_j(\bar{x}(t), t), \quad j = 1, \dots, 39 \quad (21)$$

Where $\bar{x}(t) = \{x_1(t), \dots, x_{39}(t)\}$ is the state vector of compartmental corresponding pressure, flow, and volumes which is fully discussed in Appendix A.

The corresponding set of nonlinear ODE's were solved using the ode23t MATLAB function.

2.4.2. Cardiac pacing condition

In order to simulate the coronary arterial vasodilation during cardiac pacing, the heart rate was increased to 128 bpm [11]. Besides, the left and right ventricular pressures were chosen in such a way to produce an aortic pressure of 90 mmHg [11].

The values of resistances, compliances, and inductances of each compartment in the coronary part of the circuit were again calculated using equations (1)–(3). However, the difference between the simulations of pacing and rest conditions is that in the pacing, the values of resistances, compliances, and inductances change over time until reaching a steady-state condition. It is based on the fact that by increasing the heart-beat, diameters of vessels change, due to the release of nitric oxide. Therefore, the values of resistances, compliances, and inductances change frequently. For the simulation of the cardiac pacing, the total average of LAD and LCX flows are assumed to increase by 50% of the rest condition based on the work by Quyyumi et al. [10]. Therefore, the myocardial flow is 3.3 ml/s in the left main coronary artery. Besides, it is assumed that the pressure drop in the pacing condition is 85 mmHg, which is the difference between assumed aortic pressure (90 mmHg) and venous pressure of 5 mmHg.

To the best of authors' knowledge there is no available data for resistances and compliances of the pulmonary and systemic circulatory at pacing condition. Therefore, as a first estimation, these values are assumed to be the same as ones for the resting condition. This assumption is reasonable since the aortic pressure does not considerably alter during pacing condition. Such an assumption was also used by Pagiatakis et al. [39] and Duanmu et al. [48], for the simulation of hyperemic condition.

The hemodynamics governing equations are now associated with nitric oxide vasodilation dynamical equations to predict the arterial dilation and associated increment of blood flow.

The dynamic state equations of the coronary arterial vasodilation during pacing condition, are obtained by coupling cardiovascular model and NO regulation model. This is done by converting the transfer function of NO regulation to the state-space domain. Therefore, calcium concentration, NO production rate (both calcium-dependent and calcium-independent paths), total NO concentration, and dilation transfer functions are converted to a set of ODE's for each artery and coupled to the cardiovascular dynamic model. Consequence, the following equations are obtained:

$$\frac{dx_j}{dt} = \varphi_j(\bar{x}(t), t), \quad j = 1, \dots, 182 \quad (22)$$

As mentioned, while simulating coronary vasodilation, arteries' diameters change with time and, at each time step, values of resistance, capacitance, and inductance of coronary analog network are updated and the new set of equations are solved accordingly. To carry out the simulation, oxygen partial pressure was assumed to be 95 mm Hg based on the previous study on the NO model by Wang et al. [31].

3. Results

3.1. Model validation

The velocity waveform of the left main coronary artery (LMCA) was compared with the experimental study of Davis et al. [49], and the result is presented in Fig. 3. To mimic the blood pressure measured by Davis et al. [49] (Fig. 3a) in rest condition, the model parameters were adjusted in such a way that the LMCA blood pressure of 143/82 mmHg was produced. Afterward, the velocity waveform was obtained. Fig. 3b indicates the experimental and numerical waveforms of LMCA velocity. According to this figure, the model is well able to predict a 90-degree phase difference between pressure and velocity in left coronary arteries. Also, pressure and velocity have well been predicted in both systole and diastole, in terms of both trend and value. Based on these comparisons, it can be concluded that the developed model is well able to predict pressure and velocity waveforms in left coronary arteries.

3.2. Average flow

The average inlet flow rate of all left coronary arteries and all of its branches are depicted in Fig. 4 for both baseline and pacing conditions. In the baseline condition, the average flow changes from 0.21 mL/s to 2.44 mL/s, depending on the diameter of the artery. In fact, the higher the diameter of an artery is, the more blood flow is supplied through that artery. As an example. The average flow rate of LMCA is 2.44 mL/s, while the average flow rate of LCX3 is 0.55 mL/s. Also, during cardiac pacing and for all of the branches, the flow increases until reaching a plateau level. This change is related to the release of NO that causes the arterial wall to dilate and increases the capacity of a branch to pass blood flow.

3.3. Shear stress

Fig. 5 illustrates the changes in time-average wall shear stress (TAWSS) of each heart cycle during cardiac pacing condition. According to this figure, in the coronary network, the behavior of TAWSS is biphasic, meaning that at first, the TAWSS reduces to reach a plateau level and then remains approximately constant. Based on the obtained results, the range of TAWSS changes in coronary network is from 60 to 11 dyn/cm². Also, if only consider the TAWSS in plateau, TAWSS changes from 37 to 11 dyn/cm². It should be mentioned that the higher values of TAWSS are related to the smaller branches (e.g. TAWSS ≈ 37 dyn/cm² for LCX3) and the lower values of TAWSS are related to the larger branches (e.g., TAWSS ≈ 11 – 12 dyn/cm² for LAD, LCX, and LMCA).

3.4. Dilation

In Fig. 6, the dilation percent of all coronary network is depicted versus time. As can be seen, the behavior of dilation percent of arteries is triphasic. First, the diameter of arteries increases in response to the temporal gradient of WSS. However, approximately in the first few seconds that WSS reaches the plateau, the impact of temporal shear stress on dilation percent dissipates, and thereby, the diameter of arteries reduces. Nevertheless, this reduction is not remarkable. Afterward, the diameters increase under the impact of the magnitude of WSS in plateau, and eventually the diameters become quite constant at the plateau level. While looking at the values at the plateau level, the dilation percent range changes from 8% (for LMCA) to 17% (for LCX3). It means that the dilation percent is higher for smaller arteries in comparison with larger ones.

3.5. Nitric oxide release

The amount of NO concentration during cardiac pacing is shown in

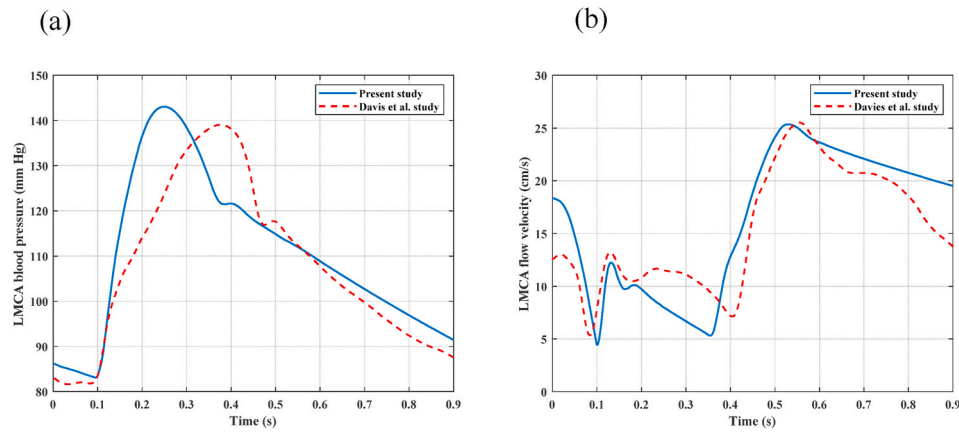


Fig. 3. The comparison between the results of the present study and the measurements of Davies et al. [49] for a) LMCA pressure and b) LMCA velocity.

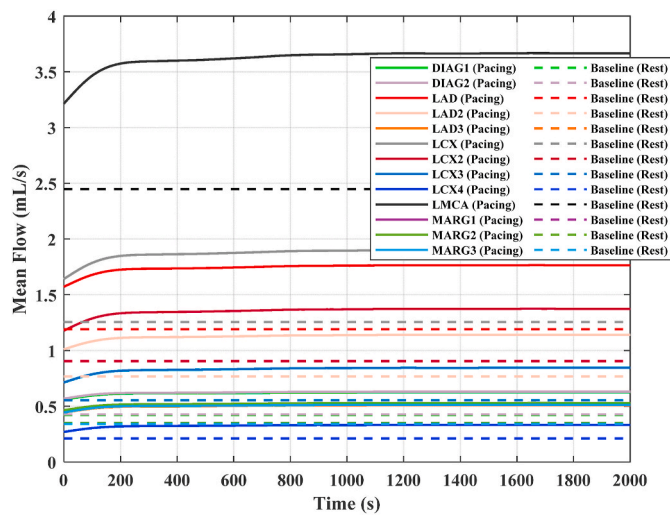


Fig. 4. Mean flow rate versus time during cardiac pacing for different branches of the coronary tree.

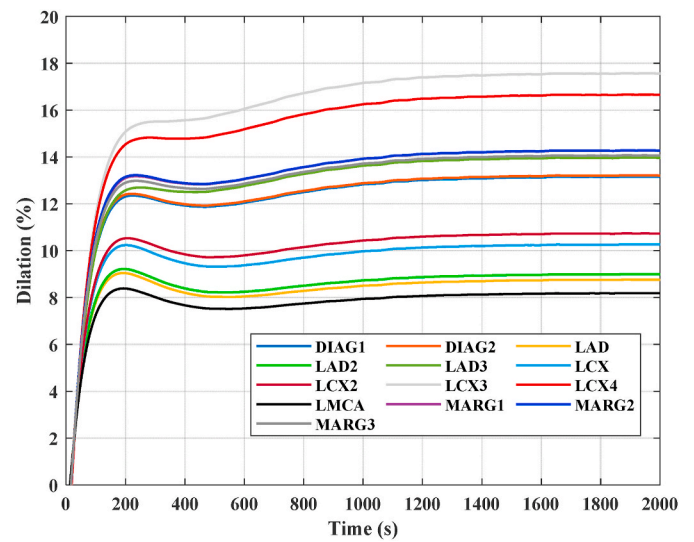


Fig. 6. Dilation percent versus time during cardiac pacing.

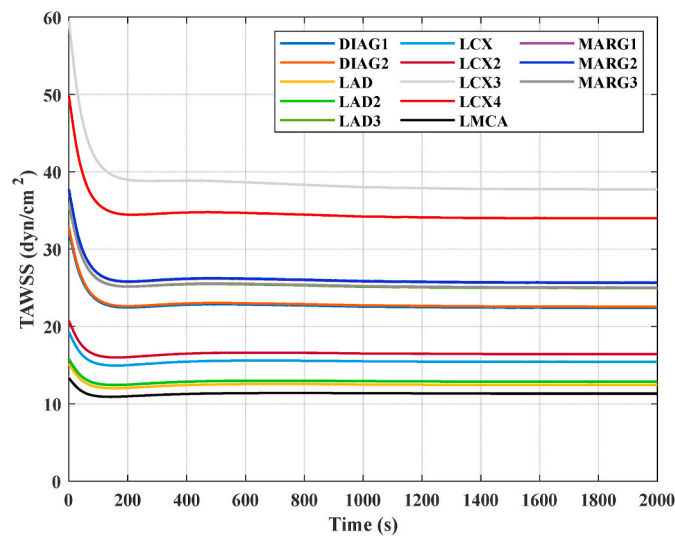


Fig. 5. Time-averaged wall shear stress (TAWSS) versus time during cardiac pacing.

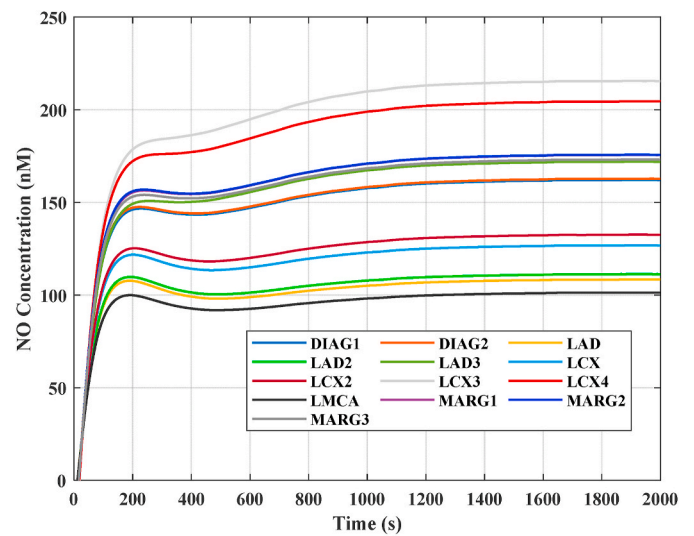


Fig. 7. NO concentration versus time during cardiac pacing.

Fig. 7. The release of NO in arteries is also triphasic that includes three different phases. First, its level increases with a slight reduction. Afterward, the level increases again and ultimately reaches a steady-state condition, called plateau. According to Fig. 7, the NO concentration in plateau changes from 100 nM to 215 nM. Also, similar to dilation percent and TAWSS, NO concentration is also higher for smaller branches. To give a sense, NO concentration is 100 nM for LMCA and 215 nM for LCX3.

3.6. Calcium concentration

The calcium concentration during cardiac pacing is demonstrated in Fig. 8. According to this figure, the behavior of Ca is biphasic; a rapid increase until reaching a peak, and then a slow decrease to reach a plateau. The Ca level is higher for smaller arteries that have higher TAWSS. In the peak, the Ca level changes from 56 nM to 77 nM, while in the plateau, the change in the range of Ca level for coronary network is less (from 17 nM to 23 nM). Based on the figure, it can be observed that both in peak and in plateau, the Ca level is higher for smaller arteries. For example, in the peak, the Ca level is 56 nM and 77 nM for LMCA and LCX3, respectively. These values change to 17 nM and 23 nM for the Ca level in plateau.

3.7. Effect of hematocrit

The dynamic viscosity of blood is 0.0035 Pa.s at its normal level [37]. In this study, the impact of changing Hematocrit from 30% to 60% was considered on the flow rate. It should be mentioned that the model that governs the hematocrit behavior is the same as the model proposed by Guyton and Hall [54]. The result of this investigation is indicated in Fig. 9, for LMCA. According to this figure, by increasing the Hematocrit, the blood flow of LMCA reduces slightly, in particular, in the relative extrema of the waveforms and also in the diastole.

Also, the impact of hematocrit was studied on the NO concentration of LMCA and the results are demonstrated in Fig. 10. According to this figure, by increasing hematocrit from 30% to 60%, the NO concentration decreases in overall. Also, NO concentration at plateau decreases from 125 nM to 78 nM, by increasing hematocrit from 30% to 60%.

4. Discussions

According to Fig. 4 the average inlet flow rate of arteries is not constant over time during cardiac pacing. It is due to the fact that the

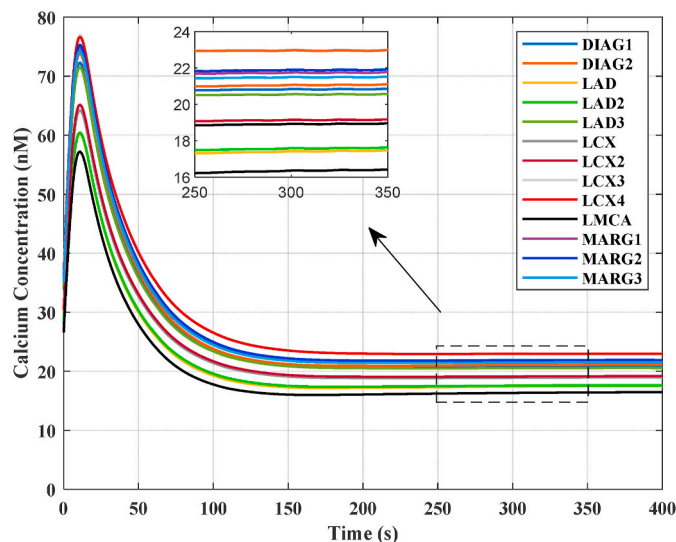


Fig. 8. Calcium concentration versus time during cardiac pacing.

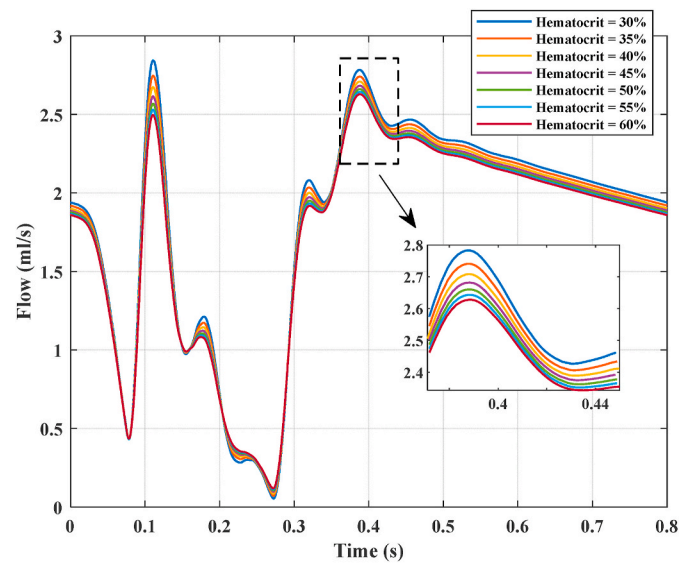


Fig. 9. The flow rate of LMCA for different hematocrits during cardiac pacing.

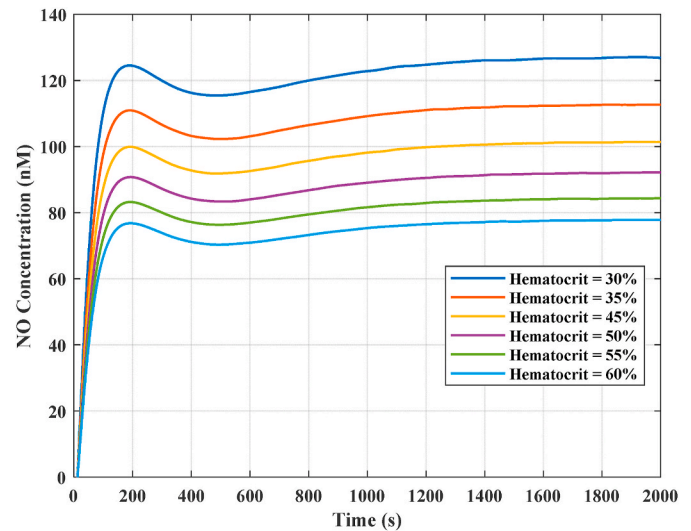


Fig. 10. NO Concentration of LMCA for different hematocrits during cardiac pacing.

gradual release of nitric oxide in arteries is considered in governing equations. As a result, the inlet flow rate of all arteries changes gradually until reaching a steady-state condition, which is consistent with what happens in reality. Also, as shown, the higher the diameter of an artery is, the more blood flow is supplied through that artery. It is because the flow rate in each artery is proportional to the third power of its diameter, based on Murray's law [52]. Moreover, according to Fig. 4, the average flow rate of LAD during the baseline condition is 1.27 ml/s. This value is in agreement with the in-vivo measurement of Gould et al. [47], meaning 1.1 ml/s, for LAD. The reason for the discrepancy between these two numbers (1.27 ml/s and 1.1 ml/s) might be due to differences in blood pressure, heart rate, different arteries' diameters, and other anatomical and physiological parameters. In addition, in the present mathematical study, the average inlet flow rate of LAD during cardiac pacing is about 1.76 ml/s, which is 38% more than that in the baseline condition. This increase is in agreement with the measurements of Nishikawa et al. [11]. Nishikawa et al., by evaluating the left anterior descending (LAD) diameter and flow rate during rest and cardiac pacing (in vivo study), have examined the function of endothelium-dependent

vascular regulation in patients with and without coronary artery stenosis. They have experimentally demonstrated that during cardiac pacing, the amount of inlet LAD flow increases 35–58% with respect to the rest condition.

Sibler et al. [53], using phase-contrast magnetic resonance angiography (PMRCA) for 18 healthy volunteers, have clinically (in vivo) shown that the wall shear stress is adversely related to the baseline diameter [53]. This is in agreement with the result of the current study in Fig. 5. It should be mentioned that the decrease in the TAWSS for smaller arteries is due to the fact that TAWSS is proportional to Q/d^3 , based on equation (5). In Fig. 4, it was seen that the volume flow rates increase before reaching the plateau for all arteries during cardiac pacing. However, because of the release of NO, diameter also increases in this phase, and the changes in Q and d are in such a way that TAWSS decreases until reaching a steady-state condition. Such a trend is in accordance with an experimental observation [54]. In fact, in this in-vitro experiment conducted on the femoral artery of a rabbit, Jen et al. [54] have shown that TAWSS decreases during regular pacing than baseline condition. Moreover, in this study, the plateau values of TAWSS for all arteries fall within the range of 10–40 dyn/cm². In the study by Malek et al. [55], it has been stated that the values of TAWSS for normal arteries (without stenosis) is approximately 10–70 dyn/cm². As a consequence, the provided model in this article could correctly calculate the value and the trend of TAWSS for coronary network.

Also, the triphasic behavior of the dilation percent of coronary network due to the effects of temporal shear and magnitude of shear was shown in Fig. 6. It has also been indicated experimentally in an in vitro study by Butler et al. [21]. In this in vitro study, Butler et al. [21] studied the impact of step and ramp-induced shear stresses on the arteriolar dilation of an excised arteriole of a rat. Moreover, in Fig. 5, it was shown that the TAWSS is higher for smaller arteries. According to Fig. 6, also, the dilation percent is higher for smaller arteries. As a result, it can be concluded that by increasing the TAWSS, the dilation percent would also increase. This is because more TAWSS releases more NO, and consequently, more dilation percent ensues [55]. This behavior is also in accordance with the in vivo study by Sibler et al. [53] that was performed on 18 healthy volunteers. Also, as stated, we used the in vivo measurements provided by Nishikawa et al. [11] and Quyyumi et al. [10], that have done on the left anterior descending (LAD) of a wide range of patients, to present a suitable mathematical equation governing the dilation percent of coronary network. According to these studies, the dilation percent for LAD artery is 8–9%. Based on this data the transfer function proposed by Lanzarone [27] was modified with 3 poles and 3 zeros to generate approximately 8–9% dilation for the LAD artery. As it can be seen in Fig. 6, the dilation for LAD is somewhere between 8 and 9%, which in turn suggests that the modified equation is well able to predict the dilation percent of the coronary network. Furthermore, as Fig. 6 indicates, the dilation percent starts from negative values which is in contrast with the physics of the problem. This is due to the iterative procedure employed to solve ODE's with arbitrary initial conditions whose effects are observed initially and diminish as convergence is achieved.

In addition, the triphasic behavior of NO, which was shown in Fig. 7 is in accordance with the in vitro measurement by Corson et al. [22] who have measured the NOx in endothelial cells of bovine aorta using bovine cultured aortic endothelial cells (BAEC) and measured NO release under different circumstances. They suggest that the trend of NOx, which is the concentration of NO's metabolites and is often measured in vivo as the indicator of NO concentration, and NO release are approximately the same. However, Luiking et al. [18] have stated that NOx may underestimate the NO production which means that NOx and NO may be different in terms of their values. Also, for smaller arteries, since they have a higher TAWSS, their NO level is higher than larger ones. Moreover, the levels of NO in plateau are in agreement with both experimental studies and previous numerical models [56,57]. For instance, according to an in vitro study by Andrews et al. [56], when WSS

increases from 0.1 dyn/cm² to 10 dyn/cm², the NO concentration in the plateau would reach 50 nM. Besides, based on the numerical study provided by Yamazaki and Kamiyama [58], when WSS changes from 5 to 13 dyn/cm², the NO concentration should fall within the range of 50–200 nM. In the current model, the value of WSS in the plateau is approximately 12 dyn/cm² and the NO level in the plateau is around 100 nM for LMCA. Taking into account the studies by Andrews et al. [56] and Yamazaki and Kamiyama [58], it can be concluded that the NO level predicted by this article is in the order of the previously reported values.

Besides, the biphasic behavior of Ca is completely in agreement with the behavior of Ca activation in experimental measurements [23,59]. In addition, the amount of Ca in peak and plateau, also, are in accordance with experimental measurements [23,59]. In this regard, Blackman et al. [23] scraped the endothelial cells of the luminal surface of the calf's ascending aorta after collagen injection and grew them in a specific media and evaluated the impact of WSS on Ca concentration in peak and plateau. According to this study, for WSS value of 10 dyn/cm², the peak value of Ca is around 20–80 nM. Also, the final concentration of Ca in the plateau is between 20 and 30 nM. In the current study and for LMCA, the steady-state value of WSS is equal to 12 dyn/cm² in cardiac pacing, and the peak and plateau Ca concentration, are 58 and 17 nM, respectively. Moreover, in the experimental study by Blackman et al. [23], the concept of recovery time was introduced which is the duration in which the Ca concentration reaches its plateau. Based on this study, the recovery time increases by increasing WSS and decreasing the diameter. As a result, it is expected that the recovery time for smaller arteries is more than that of larger ones. The result of the current study in Fig. 8, also, predicts such a behavior for recovery time.

Hematocrit has a key role in the total scavenging rate of NO. Also, the total scavenging rate of NO can highly affect the final concentration of NO. As a result, since the main focus of the study was on the investigation of NO release, hematocrit, as one of the determining factors in NO release, was also included in the study. In this study, the impact of Hematocrit on the flow rate was considered using the model proposed by Guyton and Hall [50]. The result of this investigation is indicated in Fig. 9, for LMCA. According to this figure, by increasing the Hematocrit, the blood flow of LMCA reduces. This behavior can be explained by the fact that by increasing the hematocrit, the number of red blood cells (RBCs) increases. The more RBCs in the blood, the more nitric oxide is absorbed by them, and thereby, the NO concentration in the endothelium is diminished. This can be observed from the results provided in Fig. 10. Besides, by increasing the Hematocrit, the dynamic viscosity of blood increases [51], and according to equation (5), the microvascular resistance increases. All of the aforementioned factors lead to a decrease in the blood flow rate by increasing the Hematocrit. This result is also in agreement with the recent experimental research by Hoiland et al. [16].

The present study has some limitations that should be mentioned. First of all, the blood was considered Newtonian, which might be a suitable assumption for large to medium arteries [60]. However, in reality, the blood is a non-Newtonian fluid. Second, the exact relationship between the NO concentration and elasticity is ignored in this study as it is currently unknown. Third, in the present study, the impact of NO release has only been considered for coronary arteries, though NO release affects all of the arteries which is one other limitation. However, as the aortic pressure, as the inlet boundary condition for coronary arteries in this study, remains approximately constant after the release of NO [11], it is reasonable to only consider the impact of NO release in coronary arteries and ignore its effect for the rest of arteries. Finally, for the blood pressure assumption, as we did not have access to the in vivo measurements, a pressure from the literature has been used, which is another limitation of the current study.

5. Conclusion

A dynamic model for variation of calcium and NO concentration in

the coronary artery was developed based on Lumped Parameter Models (LPM) of cardiovascular network. The main aim of this study was to mathematically model the impact of NO release in coronary arteries during cardiac pacing and its effect on hemodynamic parameters. It was seen that by increasing NO with cardiac pacing, flow rate of coronary arteries increases, while TAWSS reduces. It should be mentioned that TAWSS in plateau changes from 11 to 60 from larger arteries to smaller ones. Besides, it was observed that the behavior of dilation percent and NO concentration is triphasic while for Ca is biphasic. In this regard, by considering the values in plateau, dilation percent changes from 8 to 17%, NO concentration varies from 100 to 215 nM, and Ca concentration changes from 17 to 23 nM, all from larger arteries to smaller ones. Besides, it was observed that the behavior of dilation percent and NO concentration is triphasic while for Ca is biphasic. Finally, the impact of increasing in hematocrit during cardiac pacing was investigated on the flow waveform of LMCA. It was indicated that by increasing the Hematocrit, the blood flow of LMCA reduces. The results of this study were compared with experimental measurements to validate the model and a good agreement was observed. Such a study might lead to further researches to understand the mechanisms underlying vessel damage, and thereby to offer insights for the prevention or treatment of cardiovascular diseases.

Author contributions

Hossein Moshfegh, (MSc) developed the code and performed the computations, performed the data analysis and prepared the manuscript. Farshad Tajeddini (MSc) checked the code, and prepared the manuscript. Hossein Ali Pakravan (PhD) was the supervisor of this project and defined the research topic, advised on data analysis, and provided feedback and suggestions on the manuscript. Mojtaba Mahzoon (PhD) advised on data analysis, and provided feedback and suggestions on the manuscript. Ehsan Azadi Yazdi (PhD) was the co-advisor of this project and advised on data analysis. Hamed Bazrafshan (MD) assisted in clinical data collection, and provided feedback and suggestions on the manuscript.

Declaration of competing interest

None Declared.

Appendix A. Supplementary data

Supplementary data to this article can be found online at <https://doi.org/10.1016/j.combiomed.2021.104958>.

References

- W. He, M. Paula Kweisa, E. Gebreyesus, S. Liu, Nitric oxide and oxidative stress-mediated cardiovascular functionality: from molecular mechanism to cardiovascular disease, in: *Vascular Biology* [Working Title], IntechOpen, 2019.
- R.T. Premont, J.D. Reynolds, R. Zhang, J.S. Stamler, Role of Nitric Oxide Carried by Hemoglobin in Cardiovascular Physiology: Developments on a Three-Gas Respiratory Cycle, *Circulation Research* (2020) 129–158. Lippincott Williams and Wilkins.
- D.A. Chistiakov, A.N. Orekhov, Y.V. Bobryshev, Effects of shear stress on endothelial cells: go with the flow, *Acta Physiol.* 219 (2) (01-Feb-2017) 382–408. Blackwell Publishing Ltd.
- K. Sriram, J.G. Laughlin, P. Rangamani, D.M. Tartakovsky, Shear-induced nitric oxide production by endothelial cells, *Biophys. J.* 111 (1) (Jul. 2016) 208–221.
- H. Shimokawa, S. Godo, Nitric oxide and endothelium-dependent hyperpolarization mediated by hydrogen peroxide in health and disease, *Basic Clin. Pharmacol. Toxicol.* 127 (2) (Aug. 2020) 92–101.
- T. Roux-Mallouf, et al., Effects of acute nitric oxide precursor intake on peripheral and central fatigue during knee extensions in healthy men, *Exp. Physiol.* 104 (7) (Jul. 2019) 1100–1114.
- U. Förstermann, N. Xia, H. Li, Roles of vascular oxidative stress and nitric oxide in the pathogenesis of atherosclerosis, *Circ. Res.* 120 (4) (17-Feb-2017) 713–735. Lippincott Williams and Wilkins.
- J. yi Chen, et al., Nitric oxide bioavailability dysfunction involves in atherosclerosis, *Biomed. Pharmacother.* 97 (August 2017) (2018) 423–428.
- H. M. F. A. L. Tf, Nitric oxide in hypertension, *J. Clin. Hypertens.* 8 (12 Suppl 4) (2006) 17–29.
- A.A. Quyyumi, N. Dakak, N.P. Andrews, D.M. Gilligan, J.A. Panza, R.O. Cannon, Contribution of nitric oxide to metabolic coronary vasodilation in the human heart, *Circulation* 92 (3) (Aug. 1995) 320–326.
- Y. Nishikawa, S. Ogawa, Importance of nitric oxide in the coronary artery at rest and during pacing in humans, *J. Am. Coll. Cardiol.* 29 (1) (Jan. 1997) 85–92.
- D. Green, C. Cheetham, C. Henderson, R. Weerasooriya, G. O'Driscoll, Effect of cardiac pacing on forearm vascular responses and nitric oxide function, *Am. J. Physiol. Cell Physiol.* 283 (4) (Oct. 2002) H1354–H1360.
- M. Harold Laughlin, D.K. Bowles, D.J. Duncker, The coronary circulation in exercise training, *Am. J. Physiol. Heart Circ. Physiol.* 302 (1) (Jan. 2012) 10–23.
- D.J. Green, E.A. Dawson, H.M.M. Groenewoud, H. Jones, D.H.J. Thijssen, Is flow-mediated dilation nitric oxide mediated?: a meta-analysis, *Hypertension* 63 (2) (Feb-2014) 376–382. Lippincott Williams and Wilkins.
- A.B. Levine, D. Punihaole, T.B. Levine, Characterization of the role of nitric oxide and its clinical applications, *Cardiology* 122 (1) (Jun. 2012) 55–68.
- R.L. Hoiland, et al., Acute reductions in haematocrit increase flow-mediated dilation independent of resting nitric oxide bioavailability in humans, *J. Physiol.* 598 (19) (Oct. 2020) 4225–4236.
- E. Eroglu, H. Bischof, S. Charoensin, M. Waldeck-Weiermaier, W.F. Graier, R. Malli, Real-time imaging of nitric oxide signals in individual cells using geNOPS, in: *Methods In Molecular Biology*, vol. 1747, Humana Press Inc., 2018, pp. 23–34.
- Y.C. Luiking, M.P.K.J. Engelen, N.E.P. Deutz, Regulation of nitric oxide production in health and disease, *Curr. Opin. Clin. Nutr. Metab. Care* 13 (1) (Jan-2010) 97–104. NIH Public Access.
- Y.J. Sung, J.H. Hotchkiss, R.E. Austic, R.R. Dietert, Direct measurement of nitric oxide in headspace gas produced by a chicken macrophage cell line in a closed culture system, *Biochem. Biophys. Res. Commun.* 184 (1) (Apr. 1992) 36–42.
- S.S. Park, et al., The real-time in vivo electrochemical measurement of nitric oxide and carbon monoxide release upon direct epidural electrical stimulation of the rat neocortex, *Analyst* 140 (10) (May 2015) 3415–3421.
- P.J. Butler, S. Weinbaum, S. Chein, D.E. Lemons, Endothelium-dependent, shear-induced vasodilation is rate-sensitive, *Microcirculation* 7 (1) (Feb. 2000) 53–65.
- M.A. Corson, N.L. James, S.E. Latta, R.M. Nerem, B.C. Berk, D.G. Harrison, Phosphorylation of endothelial nitric oxide synthase in response to fluid shear stress, *Circ. Res.* 79 (5) (Nov. 1996) 984–991.
- B.R. Blackman, L.E. Thibault, K.A. Barbee, Selective modulation of endothelial cell [Ca²⁺] response to flow by the onset rate of shear stress, *J. Biomech. Eng.* 122 (3) (Jun. 2000) 274–282.
- M. Koenigsberger, R. Sauter, J.-L. Bény, J.-J. Meister, Effects of arterial wall stress on vasomotion, *Biophys. J.* 91 (5) (Sep. 2006) 1663–1674.
- Z. Wilstein, D.M. Allgood, V.L. McLure, A.C. Miller, Mathematical model of hypertension-induced arterial remodeling: a chemo-mechanical approach, *Math. Biosci.* 303 (March) (2018) 10–25.
- P.L. Kirby, D.G. Buerk, J. Parikh, K.A. Barbee, D. Jaron, Mathematical model for shear stress dependent NO and adenine nucleotide production from endothelial cells, *Nitric Oxide - Biol. Chem.* 52 (Jan. 2016) 1–15.
- E. Lanzarone, G. Casagrande, R. Fumero, M.L. Costantino, Integrated model of endothelial NO regulation and systemic circulation for the comparison between pulsatile and continuous perfusion, *IEEE Trans. Biomed. Eng.* 56 (5) (May 2009) 1331–1340.
- M.J. Kuchan, J.A. Frangos, Role of calcium and calmodulin in flow-induced nitric oxide production in endothelial cells, *Am. J. Physiol. Cell Physiol.* 266 (3 35) (1994) 3.
- A.M. Plata, S.J. Sherwin, R. Krams, Endothelial nitric oxide production and transport in flow chambers: the importance of convection, *Ann. Biomed. Eng.* 38 (9) (Sep. 2010) 2805–2816.
- S. Takarada, et al., First evaluation of real-time nitric oxide changes in the coronary circulation in patients with non-ischaemic dilated cardiomyopathy using a catheter-type sensor, *Eur. Heart J.* 31 (23) (Dec. 2010) 2862–2870.
- R. Wang, Q. Pan, W.M. Kuebler, J.K.-J. Li, A.R. Pries, G. Ning, Modeling of pulsatile flow-dependent nitric oxide regulation in a realistic microvascular network, *Microvasc. Res.* 113 (Sep. 2017) 40–49.
- Q. S, et al., Spatiotemporal transfer of nitric oxide in patient-specific atherosclerotic carotid artery bifurcations with MRI and computational fluid dynamics modeling, *Comput. Biol. Med.* 125 (Oct) (2020).
- T. Ma, et al., Flow-mediated dilation analysis coupled with nitric oxide transport to enhance the assessment of endothelial function 131 (1) (Jul. 2021) 1–14, <https://doi.org/10.1152/jappphysiol.00039.2021>.
- W.D. Haselden, R.T. Kedarasetti, P.J. Drew, Spatial and temporal patterns of nitric oxide diffusion and degradation drive emergent cerebrovascular dynamics, *PLoS Comput. Biol.* 16 (7) (Jul. 2020), e1008069.
- G. Avanzolini, P. Barbini, A. Cappello, G. Cevenini, CADCS simulation of the closed-loop cardiovascular system, *Int. J. Bio Med. Comput.* 22 (1) (Jan. 1988) 39–49.
- P.J. Scanlon, et al., ACC/AHA guidelines for coronary angiography. A report of the American college of cardiology/American heart association task force on practice guidelines (committee on coronary angiography), *J. Am. Coll. Cardiol.* 33 (6) (1999) 1756–1824.
- J.-Z. Wang, B. Tie, W. Welkowitz, J. Kostis, J. Semmlow, Incremental network analogue model of the coronary artery, *Med. Biol. Eng. Comput.* 27 (4) (Jul. 1989) 416–422.
- R. Pietrabissa, S. Mantero, T. Marotta, L. Menicanti, A lumped parameter model to evaluate the fluid dynamics of different coronary bypasses, *Med. Eng. Phys.* 18 (6) (Sep. 1996) 477–484.

- [39] C. Pagiatakis, J.C. Tardif, P.L. L'Allier, R. Mongrain, A numerical investigation of the functionality of coronary bifurcation lesions with respect to lesion configuration and stenosis severity, *J. Biomech.* 48 (12) (Sep. 2015) 3103–3111.
- [40] M. Ariane, D. Vigolo, A. Brill, F.G.B. Nash, M. Barigou, A. Alexiadis, Using Discrete Multi-Physics for studying the dynamics of emboli in flexible venous valves, *Comput. Fluids* 166 (2018) 57–63.
- [41] M. Molavi Zarandi, R. Mongrain, O.F. Bertrand, Determination of flow conditions in coronary bifurcation lesions in the context of the medina classification, *Model. Simulat. Eng.* 2012 (2012).
- [42] A. Farghadan, A. Arzani, The combined effect of wall shear stress topology and magnitude on cardiovascular mass transport, *Int. J. Heat Mass Tran.* 131 (2019) 252–260.
- [43] Y.C. Boo, H. Jo, Flow-dependent regulation of endothelial nitric oxide synthase: role of protein kinases, *Am. J. Physiol. Cell Physiol.* 285 (3 54–3) (01-Sep-2003) 499–508. American Physiological Society.
- [44] I. Fleming, R. Busse, Molecular mechanisms involved in the regulation of the endothelial nitric oxide synthase, *Am. J. Physiol. Regul. Integr. Comp. Physiol.* 284 (1 53–1) (01-Jan-2003). American Physiological Society.
- [45] K.A. Lamkin-Kennard, D.G. Buerk, D. Jaron, Interactions between NO and O₂ in the microcirculation: a mathematical analysis, *Microvasc. Res.* 68 (1) (Jul. 2004) 38–50.
- [46] H.G. Bohlen, Is the real *in vivo* nitric oxide concentration pico or nano molar? Influence of electrode size on unstirred layers and NO consumption, *Microcirculation* 20 (1) (Jan. 2013) 30–41.
- [47] K.L. Gould, Does coronary flow trump coronary anatomy? *JACC (J. Am. Coll. Cardiol.): Cardiovas. Imag.* 2 (8) (2009) 1009–1023. Elsevier Inc.
- [48] Z. Duanmu, M. Yin, X. Fan, X. Yang, X. Luo, A patient-specific lumped-parameter model of coronary circulation, *Sci. Rep.* 8 (1) (Dec. 2018) 874.
- [49] J.E. Davies, K.H. Parker, D.P. Francis, A.D. Hughes, J. Mayet, What is the role of the aorta in directing coronary blood flow? *Heart* 94 (12) (01-Dec-2008) 1545–1547. BMJ Publishing Group Ltd.
- [50] Guyton, Guyton and hall textbook of medical physiology 13 (2014) 1.
- [51] S. Jafarzadeh, A. Nasiri Sadr, E. Kaffash, S. Goudarzi, E. Golab, A. Karimipour, The effect of hematocrit and nanoparticles diameter on hemodynamic parameters and drug delivery in abdominal aortic aneurysm with consideration of blood pulsatile flow, *Comput. Methods Progr. Biomed.* 195 (2020) 105545.
- [52] D. Stephenson, A. Patronis, D.M. Holland, D.A. Lockerby, Generalizing Murray's law: an optimization principle for fluidic networks of arbitrary shape and scale, *J. Appl. Phys.* 118 (17) (Nov. 2015), 174302.
- [53] H.A. Silber, D.A. Bluemke, P. Ouyang, Y.P. Du, W.S. Post, J.A. Lima, The relationship between vascular wall shear stress and flow-mediated dilation: endothelial function assessed by phase-contrast magnetic resonance angiography, *J. Am. Coll. Cardiol.* 38 (7) (Dec. 2001) 1859–1865.
- [54] N. Jen, et al., Atrial fibrillation pacing decreases intravascular shear stress in a New Zealand white rabbit model: implications in endothelial function, *Biomech. Model. Mechanobiol.* 12 (4) (Aug. 2013) 735–745.
- [55] A.M. Malek, S.L. Alper, S. Izumo, Hemodynamic shear stress and its role in atherosclerosis, *J. Am. Med. Assoc.* 282 (21) (Dec. 1999) 2035–2042.
- [56] A.M. Andrews, D. Jaron, D.G. Buerk, P.L. Kirby, K.A. Barbee, Direct, real-time measurement of shear stress-induced nitric oxide produced from endothelial cells in vitro, *Nitric Oxide - Biol. Chem.* 23 (4) (2010) 335–342.
- [57] Y. Yamazaki, Y. Kondo, Y. Kamiyama, Estimation of shear-stress-induced endothelial nitric oxide production from flow-mediated dilation, in: 2013 35th Annual International Conference Of the IEEE Engineering In Medicine And Biology Society, EMBC, 2013, pp. 4521–4524.
- [58] Y. Yamazaki, Y. Kamiyama, Mathematical model of wall shear stress-dependent vasomotor response based on physiological mechanisms, *Comput. Biol. Med.* 45 (1) (2014) 126–135.
- [59] R.V. Geiger, B.C. Berk, R.W. Alexander, R.M. Nerem, Flow-induced calcium transients in single endothelial cells: spatial and temporal analysis, *Am. J. Physiol. Cell Physiol.* 262 (6 31) (1992) 6.
- [60] B. J, B. Jm, Comparison of Newtonian and non-Newtonian flows in a two-dimensional carotid artery model using the lattice Boltzmann method, *Phys. Med. Biol.* 52 (20) (Oct. 2007) 6215–6228.